Journal of Power Sources 196 (2011) 9931–9938

Contents lists available at SciVerse ScienceDirect

Journal of Power Sources

journal homepage: www.elsevier.com/locate/jpowsour

Experimental analysis of spatio-temporal behavior of anodic dead-end mode operated polymer electrolyte fuel cell

A. Manokaran[a,b,*], S. Pushpavanam[b], P. Sridhar[a], S. Pitchumani[a]

[a] CSIR-Central Electrochemical Research Institute-Madras Unit, CSIR Madras Complex, Taramani, Chennai 600113, India
[b] Department of Chemical Engineering, Indian Institute of Technology Madras, Chennai 600036, India

ARTICLE INFO

Article history:
Received 16 April 2011
Received in revised form 8 June 2011
Accepted 10 June 2011
Available online 25 August 2011

Keywords:
Anodic dead-end mode
Nitrogen accumulation
Spatio-temporal current distribution

ABSTRACT

During the anodic dead-end mode operation of fuel cells, the inert gases (nitrogen and water) present in the cathode side gas channel permeate to the anode side and accumulate in the anode gas channel. The inert gas accumulation in the anode decreases the fuel cell performance by impeding the access of hydrogen to the catalyst. The performance of fuel cell under potentiostatic dead-end mode operation is shown to have three distinct regions viz. time lag region, transient current region and a steady state current region. A current distribution measurement setup is used to capture the evolution of the current distribution as a function of time and space. Co- and counter-flow operations of dead-end mode confirm the propagation of inert gas from the dead-end of anode channel to the inlet of anode. Experiments with different oxidants, oxygen and air, under dead-end mode confirm that nitrogen which permeates from cathode to anode causes the performance drop of the fuel cell. For different starting current densities of 0.15 A cm^{-2}, 0.3 A cm^{-2} and 0.6 A cm^{-2} the inert gas occupies 35%, 45% and 57%, respectively of anode channel volume at the end of 60 min of dead-end mode operation.

© 2011 Elsevier B.V. All rights reserved.

1. Introduction

Low temperature polymer electrolyte fuel cells (PEFCs) are considered as an alternate power source because of their efficiency, modularity and near zero local emissions. In general, PEFCs can be operated with hydrogen fed in three modes viz. (i) once through mode, (ii) recirculation mode, (iii) dead-end mode [1]. Among these three fuel feed mechanisms, the dead-end mode operation offers high fuel utilization with minimum auxiliary power consumption. Here, a pressure regulator is employed at the anode to supply the hydrogen fuel at a constant pressure to support the electrochemical reaction. The outlet of the anode is closed with a solenoid value. In the dead-end mode operation, "inert gas molecules" of water and nitrogen, present in the humidified oxidant (air or oxygen) can permeate from the cathode to the anode. The oxygen which also crosses over from the cathode to the anode reacts with hydrogen in the anode and generates additional water molecules at the anode. These inert gas molecules accumulate in the anode chamber when the anode outlet is closed. Hydrogen transport to the catalyst is hindered in the region where these inert gases accumulate. This leads to a reduction in the effective active area available for the electrochemical reaction. The reduction in active area due to the accumulation of inert gases leads to a decrease in fuel cell performance. The performance of the fuel cell can be revived by purging the inert gas components from the anode by opening the solenoid valve.

Hikita et al. [2] experimentally analyzed the power generation characteristics of a 25 cm^2 fuel cell in dead-end mode operation. They confirmed the presence of nitrogen in the anode by analyzing the anode gas composition using a GC-TCD. In their experiment, humidified hydrogen fuel and dry air were supplied to the fuel cell. They observed the voltage to drop at 39 mV day^{-1} during the dead-end mode operation at 1 A cm^{-2}. They studied the effect of anode humidification, current density, operating pressure, membrane thickness on nitrogen crossover. Dumercy et al. [3] carried out the dead-end mode analysis in a 100 cm^2 three-cell stack. In their experiment, they did not observe any reversible voltage drop below a current density of 0.4 A cm^{-2}. Above this value, the reversible voltage drop increased with increase in current density. Lee et al. [4] investigated the performance characteristics of a 111 cm^2 PEFC in the anodic supply mode. They studied the effect of humidity and current density on the reversible voltage loss. The voltage loss rate increased with current density when water production rate was high. Authors attributed the faster voltage drop at high current densities to an increase in the back diffusion of water. Himanen et al. [5] studied the operation of a 6 cm^2 free breathing PEFC in dead-end mode by varying humidity and pressure of hydrogen in the anode compartment. The increase in hydrogen humidity

* Corresponding author at: CSIR-Central Electrochemical Research Institute-Madras Unit, CSIR Madras Complex, Taramani, Chennai 600113, India.
Tel.: +91 44 22542068; fax: +91 44 22542456.
E-mail address: nivasmano@yahoo.co.in (A. Manokaran).

0378-7753/$ – see front matter © 2011 Elsevier B.V. All rights reserved.
doi:10.1016/j.jpowsour.2011.06.103

increased the voltage drop rate. This was attributed to increased water accumulation at the anode. The increase in anode pressure decreased the voltage decay rate by increasing the water transport from anode to cathode and by decreasing the nitrogen transport from cathode to anode.

Siegel et al. [6] studied the liquid water accumulation in a 53 cm^2 PEFC in a dead-end anode using neutron imaging. Their study delineated the water accumulation in the anode and flooding in the cathode. They observed that the voltage loss under dead-end mode operation was characterized by two regions with different slopes. They concluded that the small slope region, i.e. 2 mV min^{-1} was due to nitrogen accumulation and the larger slope region, 5–8 mV min^{-1} was due to water accumulation in the anode channel. Baumgartner et al. [7] used four reference electrodes to capture the voltage distribution across the fuel cell during the dead-end mode operation. Based on the observation, they divided the entire period of dead-end mode operation into three regions. Increase of anode overvoltage was observed in the first region. The second region was attributed to the undersupply phenomenon. A combination of undersupply phenomenon and carbon corrosion defined the third region. They also observed the presence of CO_2 in the cathode exhaust during the dead-end mode operation.

Kocha et al. [8] developed a one dimensional steady state model of an anode which is fed with pure hydrogen. They estimated the nitrogen permeability by comparing the prediction of exit mole fraction of dry nitrogen with the experimentally observed values. Muller et al. [9] extended the steady state model of Kocha et al. [8] to a transient model and predicted the voltage degradation due to nitrogen accumulation by using a third order polynomial fit. This model was developed under the assumption of both negligible water accumulation and diffusion of hydrogen in the anode channel. The predicted nitrogen concentrations were compared with experimental values measured using a mass spectrometer. Siegel et al. [10] extended this work by incorporating the diffusion of hydrogen in the anode channel. This physics based voltage model predicted the two-slope recoverable voltage drop observed experimentally. Authors attributed the dilution of the hydrogen to the slow initial decay and the nitrogen blanketing for the steeper voltage drop.

Lyczkowski and Gidaspow [11] developed a one dimensional transient model of the accumulation of impurities in fuel cells in the cathode chamber which is fed with impure oxygen. They solved the convective diffusion equation using a finite difference method and predicted the spatio-temporal variation of concentration. They showed that the inert gas accumulation starts from the closed end of the cathode and propagates towards the inlet of the cathode. They compared the experimental results with prediction from a well-mixed model and a convective diffusion model.

Though reasonable efforts are made, experimentally and theoretically, to understand the process of the accumulation of inert gas molecules in the closed anode channel, experimental quantification of inert gas evolution in the anode channel has not yet been reported to the best of authors' knowledge. This study aims to quantify the spatio-temporal evolution of the inert gas in a dead-end mode operated fuel cell using a commercially available current distribution measurement setup. The various processes causing the current decay during the dead-end mode operation are delineated by systematically analyzing the effect of various design and operational parameters on the performance of a dead-end mode operated fuel cell.

2. Experimental apparatus and method

A single cell setup with an active area of 25 cm^2 was used in this study. Membrane electrode assemblies (MEAs) procured from Alfa Aesar, UK (Catalogue No. 045362) were used in the test setup. In these commercial MEAs, a ~30 μm thick membrane was sandwiched between two electrodes each having Pt loading of 0.4 mg cm^{-2}. The anode and cathode flow fields consisted of a 7-pass 5-channel parallel serpentine channels with a channel width of 0.7 mm and channel to rib ratio of 1:1. The channel depth of the parallel serpentine flow field was 1 mm unless otherwise specified. Temperature of the fuel cell was maintained at 333 K using a PID temperature controller. High pure (99.999%) dry hydrogen from a cylinder was supplied to the anode at 122 kPa (3 psig) using a pressure regulator. A solenoid valve was placed at the outlet of the anode. This solenoid valve was closed for dead-end mode operation and opened for purging the system. A needle valve was included in the downstream of the solenoid valve to regulate the hydrogen flow during the purge process. A schematic of the experimental setup is shown in Fig. 1a. The direction of the transport of various gases through the MEA is shown in Fig. 1b.

The anode gas flow rate during the purge process was maintained at about 0.1 l min^{-1}. The oxidant flow rate was regulated at 0.8 l min^{-1} by a mass flow controller. The relative humidity of air at inlet was maintained at 80%. The pressure for the cathode was set equal to atmospheric pressure at the outlet. Anode fuel, hydrogen and cathode oxidant, air were supplied in co-flow mode to the cell unless otherwise specified. A Fuel cell test station from Arbin Instruments, USA was used to characterize the polarization behavior of the fuel cell. A pressure decay leak test was performed prior to all experiments. All the experiments were repeated at least once to verify the reproducibility of the performance.

Current Scan Lin from S++, Germany was used in this study to measure the current distribution over the active area of the fuel cell. The sensor plate had 49 segments. A schematic of the sensor plate and the serpentine channel is shown in Fig. 2. Each segment area was about 0.5 cm^2. Current measuring segments were numbered parallel to the anode gas flow in co-flow operation. For co-flow operation, the hydrogen inlet was at segment no. 1, while for counter-flow operation, the hydrogen inlet was positioned at no. 49. In both the cases, oxidant inlet was at segment no. 7 and outlet was at segment no. 43. A graphite plate of 2.5 mm thickness was used to minimize the current spreading between the segments. In this 2.5 mm thick graphite plate, the ratio of through-plane resistance to in-plane resistance between segments was 0.283. The resistance along the plane being higher, current collected at each segment was confined to that segment. Experiments were carried out under the potentiostatic mode to measure current distribution under different design and operating conditions. The current sensor plate was calibrated at the operating temperature before each run. The data for each run was logged every 15 s.

3. Results and discussion

The fuel cell voltage was adjusted to a load current density of ~0.6 A cm^{-2} under dead-end mode operation at the start of the experiment. The experiment was carried out for 200 min. During the dead-end mode operation, the current density decreased from 0.6 A cm^{-2} to about 0.25 A cm^{-2} at the end of the experiment. A typical current decay of dead-end mode operated fuel cell is shown in Fig. 3a.

In this typical curve three distinct regions can be seen. Region I is characterized by the current staying constant at ~0.6 A cm^{-2} for about 12–15 min. This is called the time lag region. After the initial time lag period, the fuel cell current starts decreasing. This region II is termed the transient region. The slope of current decay curve in the transient region decreases with time. After around 100 min of operation, the fuel cell current reaches a non-zero constant value

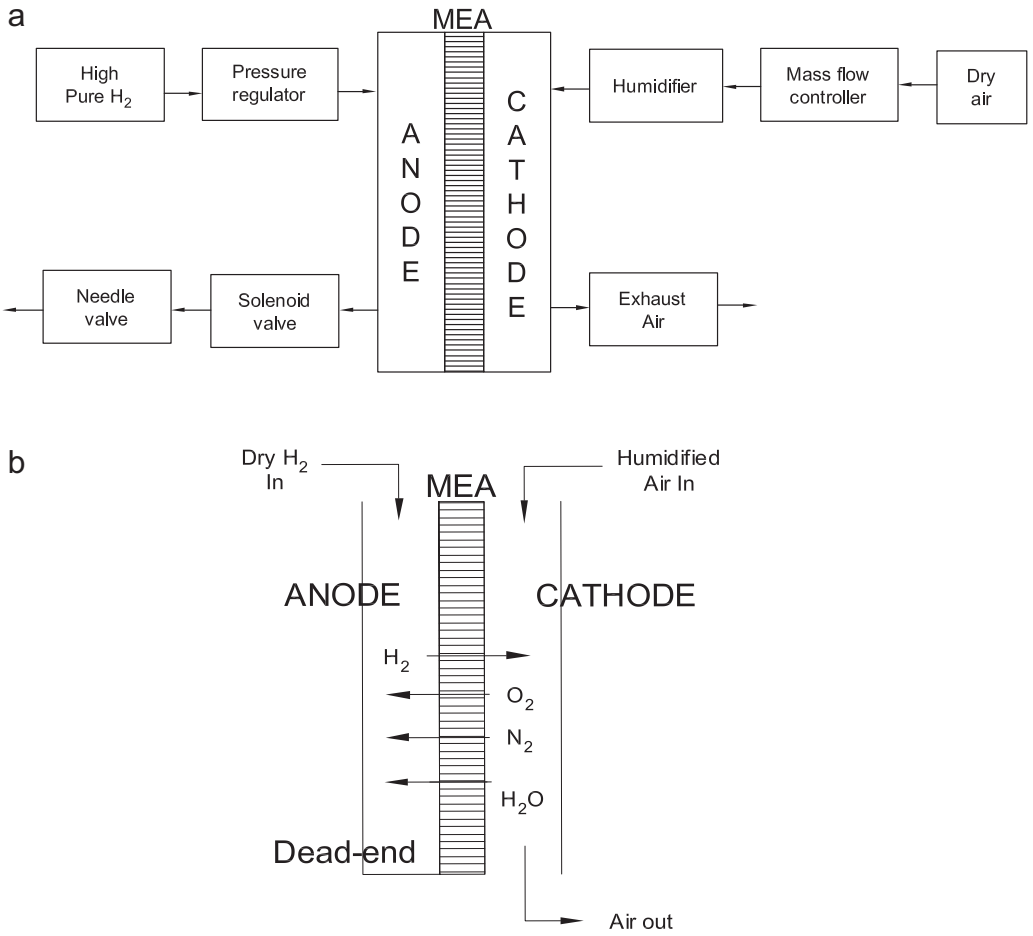

Fig. 1. (a) A schematic of experimental setup of anodic dead-end mode operation. (b) Schematic showing direction of transport of various gases through MEA.

and this is termed the steady state region. The polarization behavior of fuel cell was recorded in open mode before and after the above 200 min operation in the dead-end mode was conducted and the results are shown in Fig. 3b. It can be seen that the polarization curve recorded after 200 min operation shows an inferior performance than the performance recorded before dead-end mode operation. This is attributed to the carbon corrosion under the conditions of fuel starvation [7]. To prevent carbon corrosion, all further experiments were stopped as soon as the fuel cell current density reached the asymptotic behavior during dead-end mode operation, i.e. beginning of region III of Fig. 3a.

The cyclic transient behavior of fuel cell with an initial current density of $\sim$0.6 A cm^{-2} in dead-end mode with co-flow of reactants is given in Fig. 4a. In this test, the cell was conditioned at 0.6 A cm^{-2} for 30 min under open mode conditions. During this open mode condition, the solenoid valve was kept open and the hydrogen exhaust flow was regulated at $\sim$0.1 l min^{-1} by the needle valve. At the end of 30 min open mode operation, the solenoid valve was closed and kept at this position for 60 min. After 60 min of dead-end mode operation solenoid valve was opened and cycle was repeated. When the solenoid valve was opened, the accumulated inert gases were purged out by the fresh incoming hydrogen. This purging process rejuvenates the fuel cell and the cell instantaneously recovers its performance. Two cycles are shown, but we have tested the system up to three cycles with different MEAs. In all cases cyclic operation was observed without any loss in performance. The polarization behavior of fuel cell was recorded in open mode before and after the cyclic operation

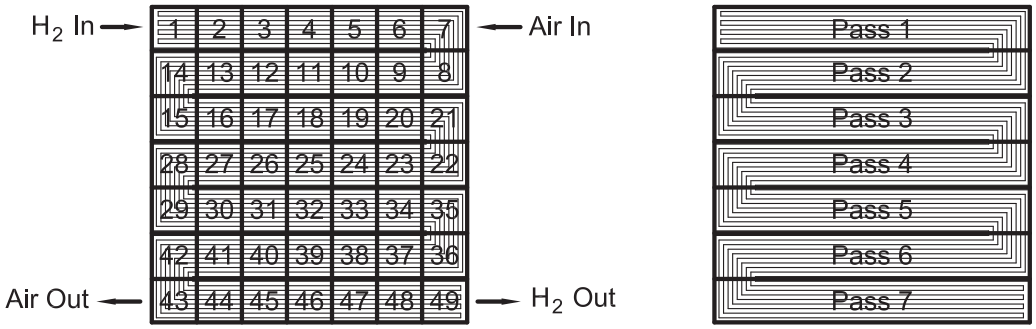

Fig. 2. Schematic of the current sensor plate and the serpentine flow-field.

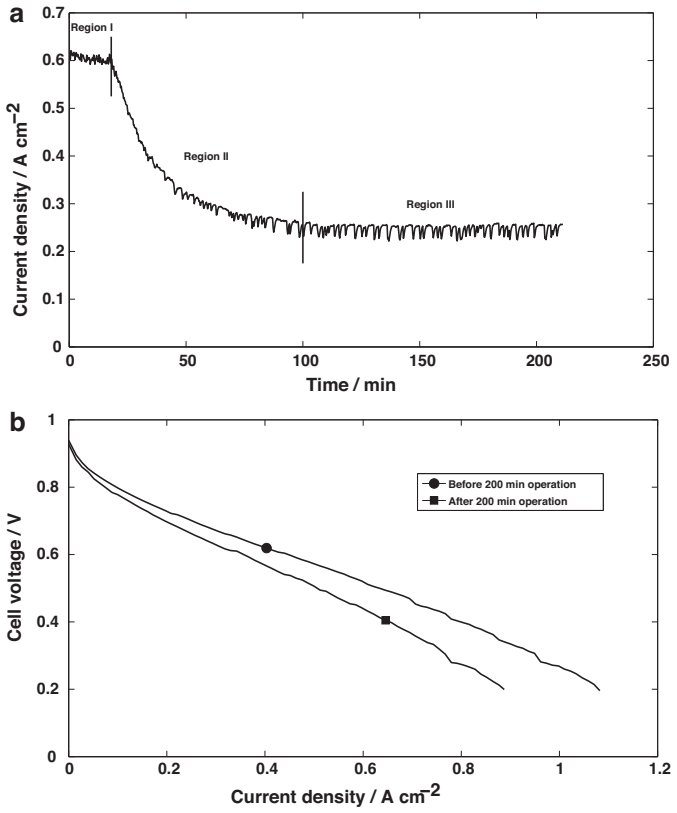

Fig. 3. (a) Typical dead-end mode response, evolution of current with time. (b) Polarization curve of fuel cell before and after 200 min of dead-end mode operation.

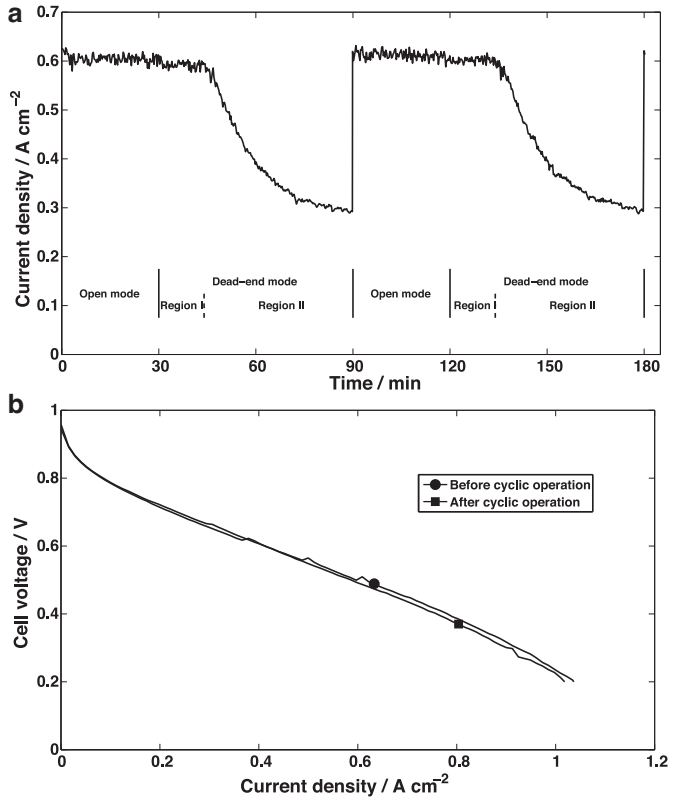

Fig. 4. (a) Cyclic transient behavior of dead-end mode operated fuel cell. (b) Polarization curve of fuel cell before and after two cycles of dead-end mode operation.

in the dead-end mode was conducted. The two curves are identical confirming there is no degradation in the characteristics of fuel cell (Fig. 4b).

For a detailed parametric analysis, the performance of the fuel cell during one cycle of dead-end mode is compared and analyzed. The spatial distributions of normalized current density at various time instants during the transient current region for co- and counter-flows are shown in Fig. 5a. The current densities are normalized with respect to the current density generated at the start of dead-end mode. The current distribution measurement in the 7×7 matrix is "straightened" and presented as a 1×49 matrix. The spatio-temporal plot of co- and counter-flow operation shows that the current density decreases first in segments near the anode outlet and this propagates to inlet of the anode. This behavior reveals that the inert gases accumulate first near the dead-end of the anode channel and propagate towards the inlet irrespective of the fuel inlet position.

The current density generated in each pass is determined by summing the current densities generated in the seven segments of a pass. This is normalized by the current density generated at the start of the transient current region. This is plotted in Fig. 5b for a time interval of 3 min. It can be seen from Fig. 5b that the drop in performance is first observed in the last pass, near the dead-end and the performance deterioration propagates with time towards the inlet. Performance deterioration of the passes near the inlet is observed before the deterioration of the last pass is complete. This indicates that the drop in performance does not propagate as a sharp boundary but as a diffused boundary. Lyczkowski and Gidaspow [11] also observed a similar S-shaped curve in their work. They attributed the lack of sharpness in the propagation front to molecular diffusion of inert gases.

The space between the successive curves represents the volume fraction occupied by the inert gas molecules during that time interval. It can be seen clearly that the space between the successive curves is less in the later part as compared to the initial stages. This indicates the decreased net flow of inert gas from the cathode to the anode as time progresses in the dead end mode operation. The decrease in net inert gas flow is due to back diffusion of inert gas from anode to cathode. At the start of the transient region, the inert gas concentration in the anode channel is negligible. Permeation of inert gas from the cathode to the anode proceeds as long as the concentration of inert gas in the cathode is greater than the concentration of inert gas in the anode. The concentration of inert gas in the anode can be higher than that in the cathode due to the electrochemical reaction as the hydrogen fuel is consumed while current is generated. As a result of this, the portion of the anode near the dead-end has high concentration of inert gas compared to the cathode. This induces a back diffusion of inert gas from anode to cathode. In steady state region of Fig. 3a, the back diffusion of inert gas from anode to cathode is equal to the permeation of inert gas from cathode to anode. Because of the zero net inert gas flow from cathode to anode, no further electrode area is blanketed and no decrease in performance is observed in the steady state region.

3.1. Effect of oxidant

Nitrogen and water are the only possible inert gases that can accumulate in the dead-end anode channel and cause deterioration in performance. To delineate the contribution of these two species to the reversible drop in fuel cell performance, dead-end mode experiments were carried out with two starting current densities of 0.6 A cm^{-2} and 0.3 A cm^{-2} using air and oxygen as an oxidant. In all experiments, oxidant flow rate and relative humidity were maintained at 0.8 l min^{-1} and 80%, respectively. The dead-end mode

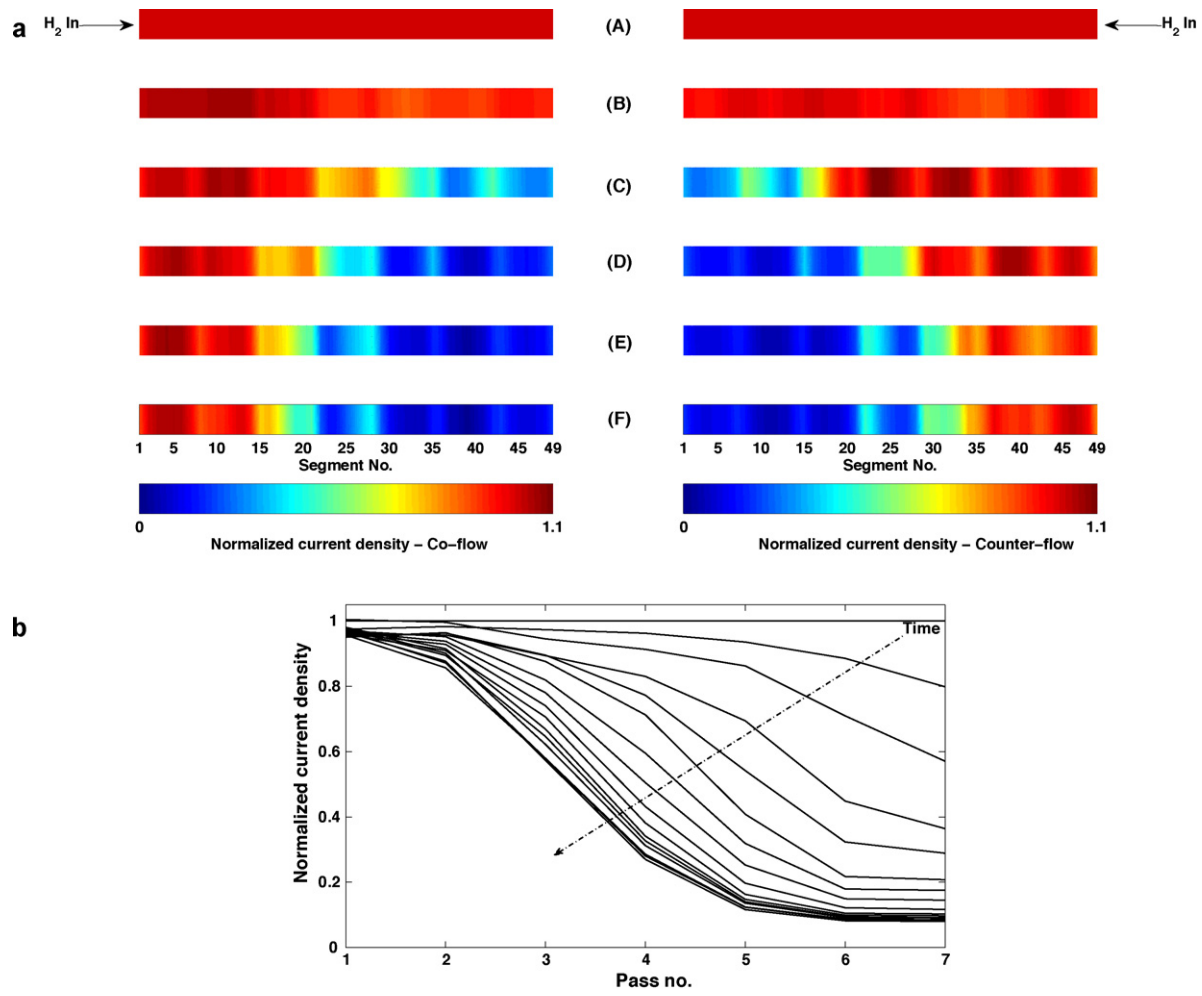

Fig. 5. (a) Spatial distribution of normalized current density at various time instants for co- and counter-flow operation (A) $t = 0$ min; (B) $t = 12$ min; (C) $t = 24$ min; (D) $t = 36$ min; (E) $t = 48$ min; (F) $t = 60$ min. (b) Variation of normalized current density for co-flow operation in different passes at a time interval of 3 min.

performance of fuel cell with different oxidants is shown in Fig. 6. When oxygen is used as an oxidant no appreciable decrease in fuel cell current density is observed. But when air is used as an oxidant the initial current density of 0.6 A cm^{-2} reduced to 0.3 A cm^{-2} and the initial current density of 0.3 A cm^{-2} reduced to 0.17 A cm^{-2} in 60 min. This experiment confirms that in the tested period, nitrogen crossover followed by its accumulation is the primary cause of the decrease in fuel cell performance and it is not water accumulation in the anode.

3.2. Effect of anode channel depth

To study the effect of flow field design on the performance of dead-end mode operated fuel cell, two different channel depths of 1 mm and 0.5 mm anode flow field plates were employed. The transient behavior of fuel cell under dead-end mode for these different channel depths of flow field is shown in Fig. 7. The anode channel volume for 1 mm and 0.5 mm channel depths is ~1.25 ml and ~0.625 ml, respectively. The experimental results show that there

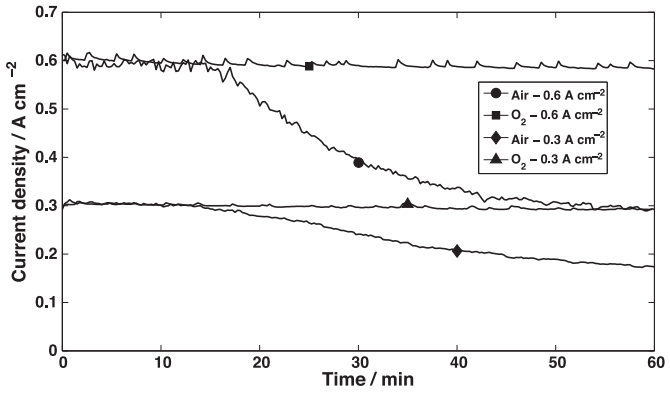

Fig. 6. Comparison of dead-end mode operation with oxygen and air as an oxidant at two different initial current densities.

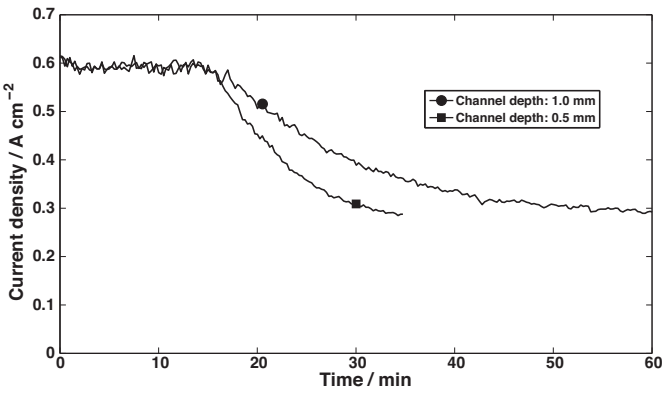

Fig. 7. Effect of channel depth on dead-end mode performance.

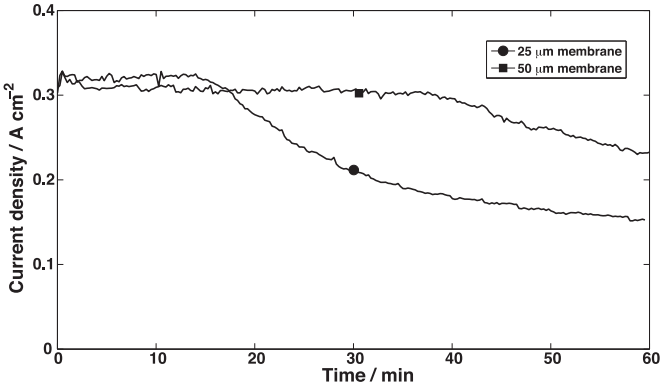

Fig. 8. Effect of membrane thickness on dead-end mode performance.

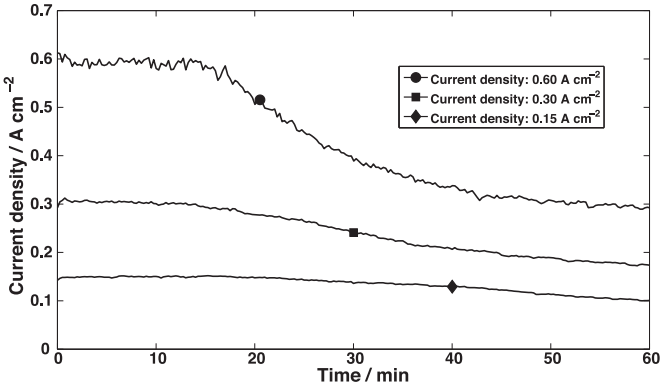

Fig. 9. Effect of different starting current densities on dead-end mode performance.

is no change in time lag when the channel volume decreases. In the transient current region, the current decay rate is higher for a 0.5 mm channel depth flow field plate as compared to a 1 mm channel depth flow field plate. The inert gas permeation rate is constant for a given membrane and operating conditions. So when the channel volume decreases, the partial pressure of the inert gas increases and it blankets more surface area quickly which leads to a rapid decrease in fuel cell performance.

3.3. Effect of membrane thickness

To find the effect of membrane thickness, two different Nafion membranes (NRE 211 and NRE 212) were sandwiched between commercial electrodes. The thickness of the NRE 211 and NRE 212 membranes are 25 μm and 50 μm, respectively. The transient response of dead-end mode operated fuel cell for a starting current density of 0.3 A cm^{-2} is shown in Fig. 8. As the thickness of the membrane is doubled, the time lag of dead-end mode operated fuel cell increased from 14 min to 37 min. From Figs. 7 and 8, it is concluded that the time lag is sensitive to the membrane thickness and insensitive to the channel volume. This clearly indicates that the time delay period is a membrane characteristic.

3.4. Effect of current density

To study the effect of operating conditions, dead-end mode experiments were carried with different starting current densities of ~0.15 A cm^{-2}, ~0.3 A cm^{-2} and ~0.6 A cm^{-2} using air as an oxidant and the results are shown in Fig. 9.

These current densities reach constant steady state values of ~0.1 A cm^{-2}, ~0.175 A cm^{-2} and ~0.3 A cm^{-2} at the end of 60 min of dead-end mode operation respectively. The different starting

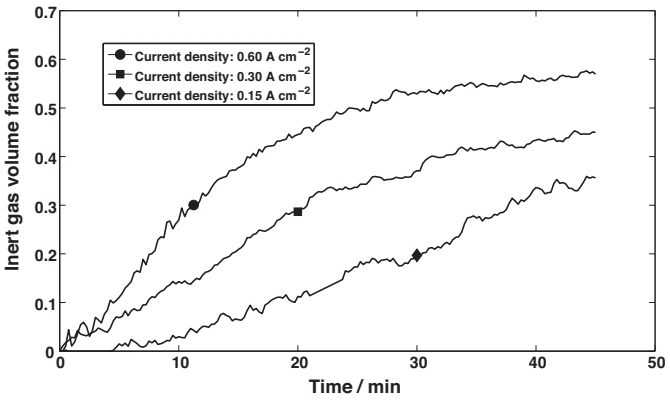

Fig. 10. Evolution of inert gas volume fraction in the anode channel at different starting current densities.

current densities approach their respective steady state values at different current decay rates. High starting current densities decay rapidly compared to low starting current densities. As mentioned earlier, the drop in fuel cell performance is due to the non availability of fuel at the catalyst sites which is in turn due to the accumulation of the inert gas. To compare the fuel cell performance across different starting currents with different current decay rates, the volume fraction/areal fraction of inert gas accumulated during the transient current region is determined. In this work, the volume fraction of inert gas in the anode channel is treated as equivalent to the areal fraction of the MEA covered with inert gas as the anode channel depth is uniform. This gives

Volume fraction of inert gas in the anode channel

$$= \text{areal fraction of the MEA covered with inert gas}$$

$$= 1 - \text{areal fraction of the MEA accessible to the fuel}$$

$$= 1 - \frac{\sum_{i=1}^{49} (I_i(t)/I_i(\text{ref}))}{49} \quad (1)$$

Here, I_i (t) is the current density generated in the ith segment at time't'. I_i (ref) is the current density generated in the ith segment at the start of the transient region (i.e. the end of the lag region). Eq. (1) is valid under the assumption that the current generation is uniform in each active segment and varies linearly with reactant mole fraction. The evolution of inert gas in the anode channel volume is shown in Fig. 10. It is observed that the initial rate of inert gas coverage is higher at high starting current densities. High starting current densities produce relatively high amount of water in the cathode compared to low starting current densities. This increases the water content in the membrane which eventually leads to the high permeation rate of nitrogen compared to the case when the starting current density is low [12,13]. At high current density, oxygen consumption rate is also high. Consequently nitrogen mole fraction is higher in cathode compared to the case of low current density. This also leads to the high permeation rate of nitrogen and subsequently faster decay rate with high starting current densities. Volume fraction of anode channel covered by the inert gas reaches the values of 35%, 45% and 57% for the starting current densities of 0.15 A cm^{-2}, 0.3 A cm^{-2} and 0.6 A cm^{-2}, respectively. The inert gas volume fraction (areal fraction) values indicate that for the starting current density of 0.6 A cm^{-2}, the inert gas permeation from cathode to anode through 43% of MEA (area which is not covered by inert gas) is compensated by the back diffusion of inert gas through 57% of MEA (area which is covered with inert gas). Similarly, for the starting current densities of 0.3 A cm^{-2} and 0.15 A cm^{-2}, 55% and 65% of the MEA is uncovered by the inert gas respectively. The diffusion of inert gas from this portion is compensated by the back

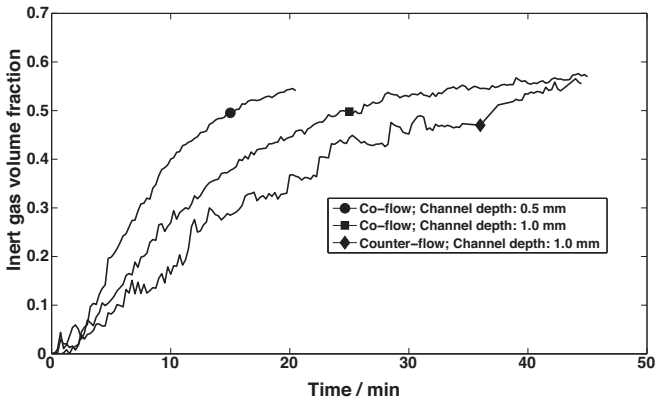

Fig. 11. Evolution of inert gas volume fraction in the anode channel under different conditions at 0.6 A cm^{-2}.

diffusion of inert gas from the 45% and 35% area of MEA which is covered by the inert gas. The mole fraction of nitrogen in the inert gas occupied region of anode is approximately unity. Taking into the consideration the oxygen consumption and the water production in the cathode, the nitrogen mole fraction in the cathode exit is found to be around 0.65 for different current densities. The procedure to calculate the nitrogen mole fraction is explained in Appendix A. In the inert gas covered region, the difference in the nitrogen mole fraction across the MEA is almost same (~0.35) at different operating current densities. Besides, no water is produced in the inert gas covered regions so that the membrane permeability is not altered. Because of the existence of similar local operating conditions and the gas compositions, the permeability of the inert gas and its flux through the membrane in the inert gas covered region is constant for the tested current densities. In the active fraction of the cell, the permeation of the inert gas from cathode to anode is higher due to the higher production of water. To compensate this, the areal fraction covered by the inert gas in the anode is higher at high current densities.

The volume fraction of inert gas for a starting current density of 0.6 A cm^{-2} under co-flow mode, counter-flow mode and for different channel depths was calculated. This is shown in Fig. 11. The rate at which the inert gas accumulates in the channel is different for different operating and design parameters. This can be seen from the slopes of the curve but the volume fraction of inert gas in the anode channel at the end of the experiment is constant. Comparison of Figs. 10 and 11 indicates that the inert gas volume fraction is largely dictated by the operating current density.

4. Conclusions

In this work the propagation of the inert gas from the end of anode channel to the anode inlet is captured using a current sensor plate under potentiostatic mode. Co- and counter-flow operations of dead-end mode confirm the reversible drop in cell voltage is solely due to inert gas accumulation. An experiment is conducted with oxygen as an oxidant. This indicates that nitrogen is the major contributor to the drop in cell performance during dead-end mode operation when air is used as an oxidant. Experiments using different depths of anode flow field channel and different thickness of membrane identified the initial time lag in the transient response of fuel cell under dead-end mode as a characteristic property of the membrane. The reason for the high decay rate with higher current density compared to the lower current density is elaborated by calculating inert gas volume fraction in the anode channel. Finally, the spatio-temporal data generated in this work can be used as a benchmark data to compare and evaluate the modeling results pertaining to the dead-end mode operation.

Acknowledgements

This work was supported by CSIR, New Delhi through a supra institutional project under EFYP.

CSIR-Central Electrochemical Research Institute assisted in meeting the publication costs of this article.

Appendix A. Nitrogen mole fraction calculation

At the dead-end portion of the anode, the mole fraction of nitrogen is assumed to be unity.

Calculation of cathode side nitrogen mole fraction:

In all experiments, the inlet dry air flow rate is regulated at 0.8 slpm. This dry air is humidified and then supplied to fuel cell with a relative humidity of 80%, at a temperature (T) of 333 K and pressure (P) of 1 atmosphere. Taking into account the mole fraction of oxygen (nitrogen) in dry air to be 0.21 (0.79), molar flow rate (MFR) of different gases is calculated in mol s^{-1}.

$$\text{Oxygen inlet dry MFR} = \frac{0.8 \times 0.21}{60} \times \frac{\text{density of oxygen (g l}^{-1})}{\text{mol. wt. oxygen (g mol}^{-1})} \quad (A.1)$$

$$\text{Nitrogen inlet dry MFR} = \text{oxygen inlet dry MFR} \times \frac{0.79}{0.21} \quad (A.2)$$

$$\text{Total inlet dry MFR} = \text{oxygen inlet dry MFR} + \text{nitrogen inlet dry MFR} \quad (A.3)$$

$$\text{Saturation pressure } (P_{\text{sat}}) = 10^{\{-2.1794+0.02953(T-273)-9.1837\times10^{-5}(T-273)^2+1.4454\times10^{-7}(T-273)^3\}} \quad (A.4)$$

$$\text{Mole fraction of water} = \frac{RH}{100} \times \frac{P_{\text{sat}}}{P} \quad (A.5)$$

$$\text{Water inlet MFR} = \text{total inlet dry MFR} \times \frac{\text{mole fraction of water}}{1 - \text{mole fraction of water}} \quad (A.6)$$

$$\text{Water production} = \frac{I \times A}{2 \times 96485} \quad (A.7)$$

'I' is the cell current in A cm^{-2}; 'A' is the cell active area in cm^{-2}.

$$\text{Water exit total MFR} = \text{water inlet MFR} + \text{water production} \quad (A.8)$$

$$\text{Oxygen exit dry MFR} = \text{oxygen inlet dry MFR} - \frac{I \times A}{4 \times 96485} \quad (A.9)$$

$$\text{Nitrogen exit dry MFR} = \text{nitrogen inlet dry MFR} \quad (A.10)$$

$$\text{Nitrogen wet exit molefraction} = \frac{\text{nitrogen exit dry MFR}}{\text{oxygen exit dry MFR} + \text{nitrogen exit dry MFR} + \text{water exit total MFR}} \quad (A.11)$$

For the starting current density of 0.15 A cm^{-2}, the steady state current density value (I) is 0.1 A cm^{-2}. For 25 cm^2 fuel cell, the cathode exit nitrogen mole fraction in wet basis is 0.659.

References

[1] F. Barbir, PEM Fuel Cells: Theory and Practice, Elsevier Academic Press, USA, 2005, p. 59.
[2] S. Hikita, F. Nakatani, K. Yamane, Y. Takagi, JSAE Rev. 23 (2002) 177–182.
[3] L. Dumercy, M.C. Pera, R. Glises, D. Hissel, S. Hamandi, F. Badin, J.M. Kauffmann, Fuel Cells 4 (4) (2004) 352–357.
[4] Y. Lee, Y.H. Jang, T. Jang, J.T. Chang, Y. Kim, ECS Trans. 3 (1) (2006) 871–878.
[5] O. Himanen, T. Hottinen, S. Tuurala, Electrochem. Commun. 9 (2007) 891–894.
[6] J.B. Siegel, D.A. McKay, A.G. Stefanopoulou, D.S. Hussey, D.L. Jacobson, J. Electrochem. Soc. 155 (11) (2008) B1168–B1178.
[7] W.R. Baumgartner, P. Parz, S.D. Fraser, E. Wallnofer, V. Hacker, J. Power Sources 182 (2008) 413–421.
[8] S.S. Kocha, J.D. Yang, J.S. Yi, AIChE J. 52 (5) (2006) 1916–1925.
[9] E.A. Muller, F. Kolb, L. Guzzella, A.G. Stefanopoulou, D.A. Mckay, J. Fuel Cell Sci. Technol. 7 (2010) 021013–21021.
[10] J.B. Siegel, S.V. Bohac, A.G. Stefanopoulou, S. Yesilyurt, J. Electrochem. Soc. 157 (7) (2010) B1081–B1093.
[11] R.W. Lyczkowski, D. Gidaspow, AIChE J. 17 (5) (1971) 1208–1214.
[12] C. Mittelsteadt, M. Umbrell, Proceedings of the 207th Electrochemical Society Meeting on Gas Permeability in Perfluorinated Sulfonic Acid Polymer Membranes, Toronto, Canada, May 15–20, 2005.
[13] K.D. Baik, M.S. Kim, Int. J. Hydrogen Energy 36 (2011) 732–739.